Supplementary Information

Visible Light-Promoted Nickel-NHC Photocatalysts for Free Radical Photopolymerization and 3D Printing Application

Naralyne M. Pesqueira[a,b], Fabrice Morlet-Savary[b,c], Michael Schmitt[b,c], Valdemiro P. Carvalho-Jr[a], Beatriz E. Goi,[a,*] Jacques Lalevée[b,c,*]

[a]*Faculdade de Ciências e Tecnologia, UNESP – Univ. Estadual Paulista, CEP 19060-900, Presidente Prudente, SP, Brazil*

[b]*Université de Haute-Alsace, CNRS, IS2M UMR 7361, F-68100 Mulhouse, France*

[c]*Université de Strasbourg, F-67000 Strasbourg, France*

*Correspondence to :

Jacques Lalevée (e-mail : jacques.lalevee@uha.fr)

Beatriz E. Goi (e-mail: beatriz.goi@unesp.br)

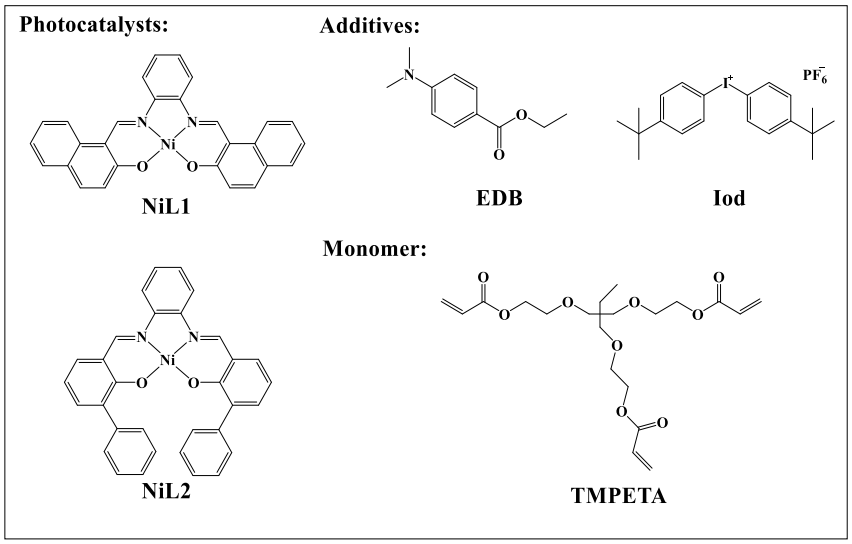

Scheme S1. Three-component system for the photopolymerization of an acrylate monomer with Ni^{II} complexes bearing Schiff base ligands as photocatalysts.[1]

Analyses

The ^{1}H NMR spectra were acquired in CD_3OD at 298 K on an Agilent MR 400 Ultrashield spectrometer operating at 400 MHz. Chemical shifts were reported in ppm relative to the high frequency of TMS. Infrared spectra were obtained on a Perkin Elmer Frontier instrument equipped with a diamond ATR module, collected between 4000 and 250 cm^{-1} at a scan rate of one spectrum every 64 s with a 2 cm^{-1} resolution at 298 K. The mass analyses have been made on a Q-TOF mass spectrometer Impact II Bruker equipped with a ESI source used in positive mode. Source parameters are settled as follow: capillary voltage at 4.5kV, nebulizer pressure at 5.8 psi (ie 0.4 bar), dry gas flow at 4.0L/min. and dry temperature at 180°C. The TOF was calibrated just before analysis using a formates sodium adducts mixture in ultra-pure water infused directly into the source in the same conditions. The sample was diluted in CH_3CN in order to reach a concentration of about 1-10ng/µL and was directly infused into the source. MALDI-

TOF analyses were performed on a Bruker Daltonics Autoflex III Smartbeam. Electronic spectra were recorded on a Shimadzu model UV-1800 spectrophotometer using 1 cm path length quartz cells. Solutions of the complexes and ligands in CH_2Cl_2 at a concentration of 2×10^{-4} mol L^{-1} were used for these measurements. Elemental analyses were conducted using a Perkin-Elmer CHN 2400 instrument.

1. ^{1}H NMR characterization of NHC ligands

HC1: Yield: 75%. ^{1}H NMR (400 MHz, $CDCl_3$, ppm, 25 °C): δ = 11.29 (t, $^4J_{H,H}$ = 1.57 Hz, 1H, NCHN), 9.15 (d, $^3J_{H,H}$ = 8.31 Hz, 1H, Ar-py), 8.80 (t, $^3J_{H,H}$ = 1.80 Hz, 1H, ImH), 8.53-8.48 (m, 1H, Ar-py), 8.07 (dt, $^4J_{H,H}$ = 1.81 Hz, $^3J_{H,H}$ = 8.04 Hz, 1H, Ar-py), 7.49-7.45 (m, 1H, Ar-py), 7.38 (t, $^3J_{H,H}$ = 1.60 Hz, 1H, ImH), 7.02 (s, 2H, Ar-mes), 2.32 (s, 3H, CH_3-Ar-mes), 2.16 (s, 6H, CH_3-Ar-mes).

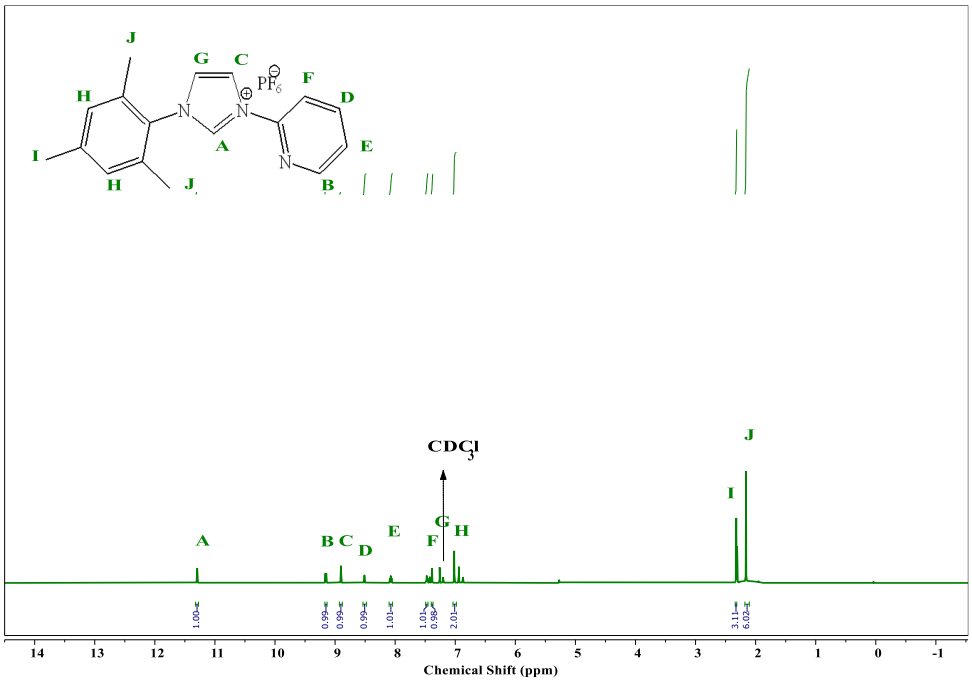

Figure S1. ^{1}H NMR spectrum for **HC1** in $CDCl_3$.

HC2: Yield: 75%. ^{1}H NMR (400 MHz, DMSO-d6, ppm, 25 °C): δ= 10.04 (t, $^{4}J_{H,H}$ = 1.50 Hz, 1H, NCHN), 8.65 (t, $^{3}J_{H,H}$ = 1.74 Hz, 1H, ImH), 8.20 (t, $^{3}J_{H,H}$ = 1.70 Hz, 1H, ImH), 7.95-7.89 (m,c 2H, *o*-ph), 7.75-7.59 (m, 3H, *m*- and *p*-ph), 2.35 (s, 3H, CH_3-Ar-mes), 2.12 (s, 6H, CH_3-Ar-mes).

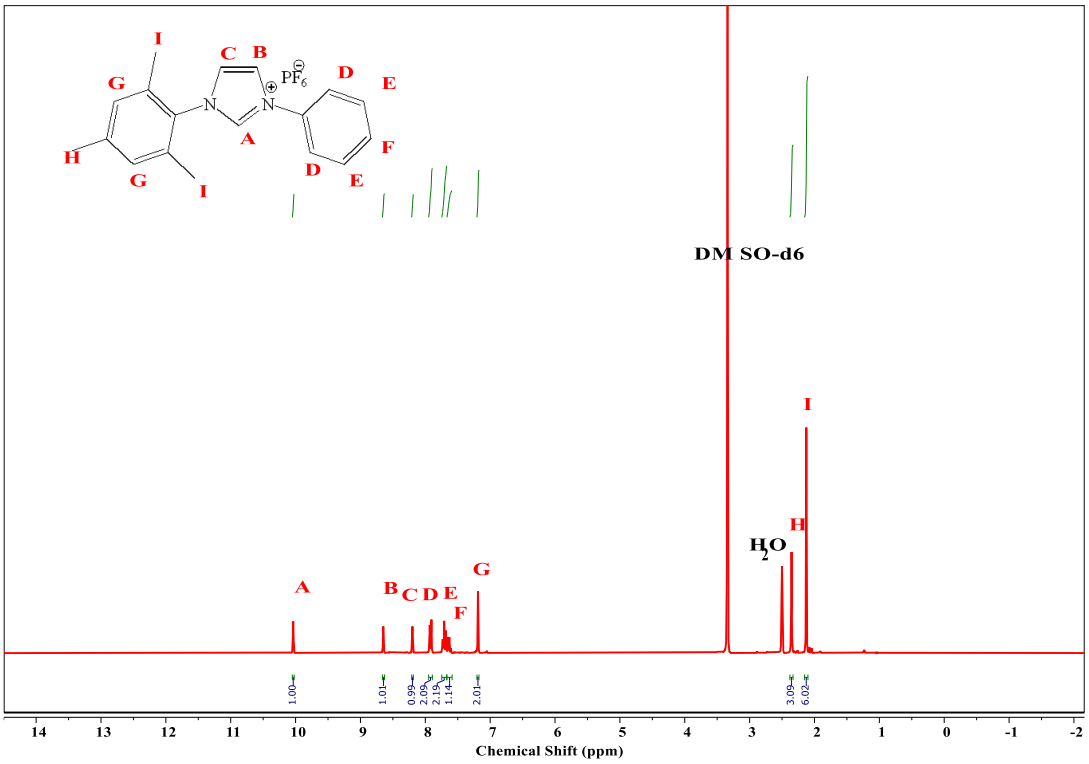

Figure S2. ^{1}H NMR spectrum for **HC2** in DMSO-d6.

2. ^{1}H NMR characterization of Ni^{II} complexes

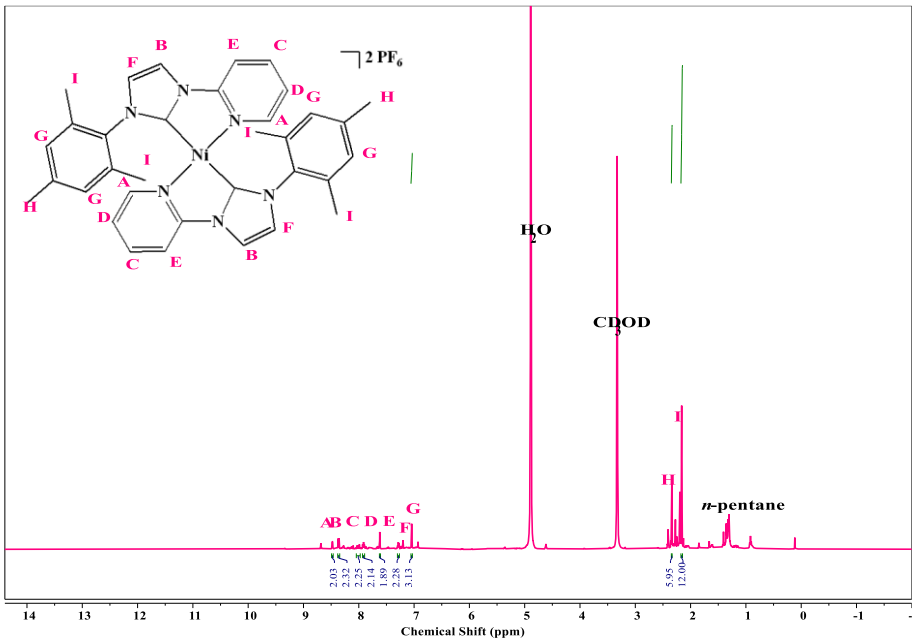

Figure S3. ^{1}H NMR spectrum for **NiC1** in CD_3OD.

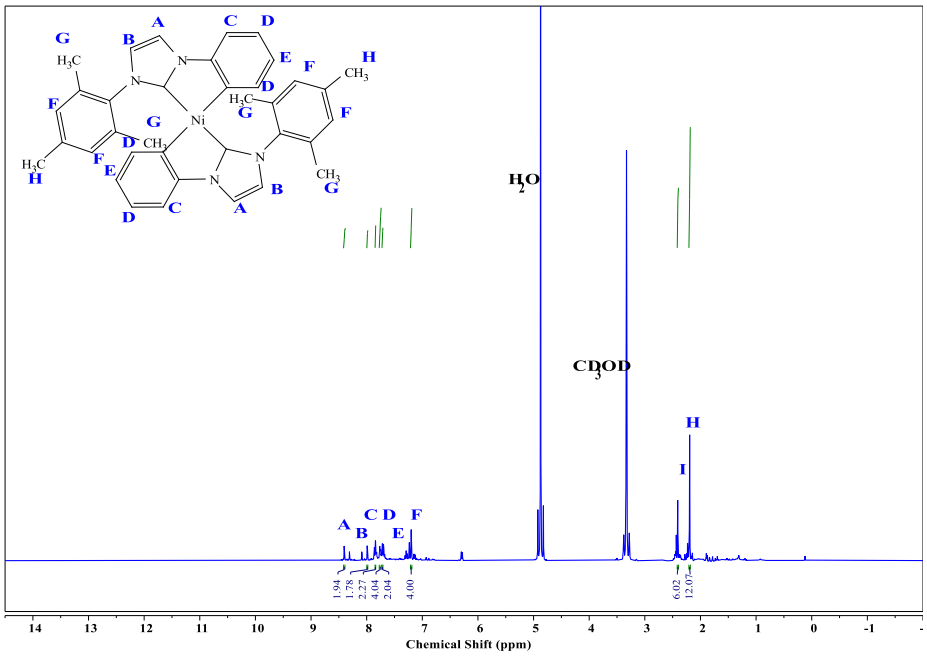

Figure S4. ^{1}H NMR spectrum for **NiC2** in CD_3OD.

3. FTIR characterization of NHC ligands and Ni^{II} complexes

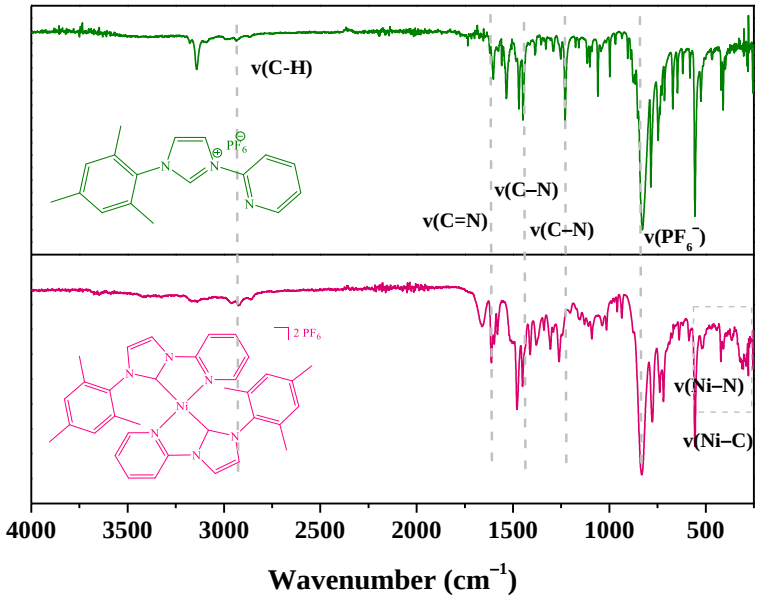

Figure S5. FTIR spectra for **NiC1** (pink line) and **HC1** (green line).

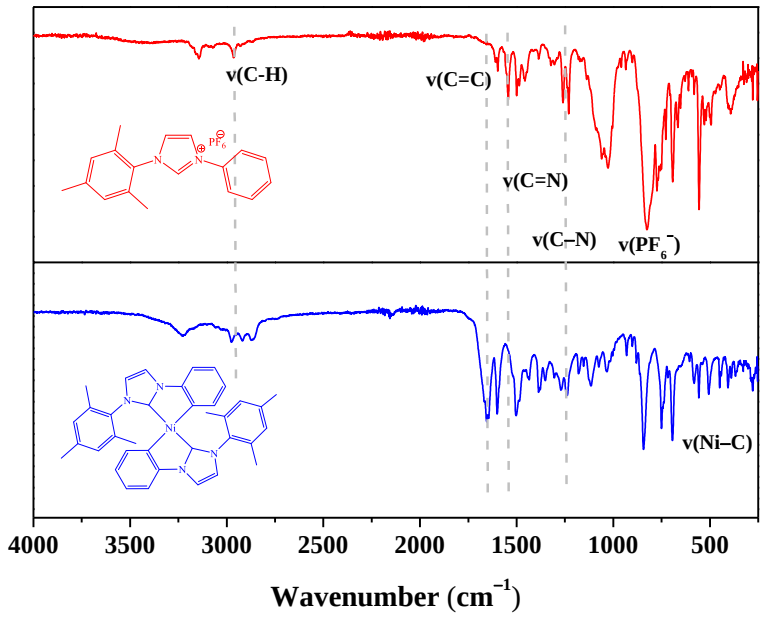

Figure S6. FTIR spectra for **NiC2** (blue line) and **HC2** (red line).

4. Experimental ESI–MS characterization of NiC1

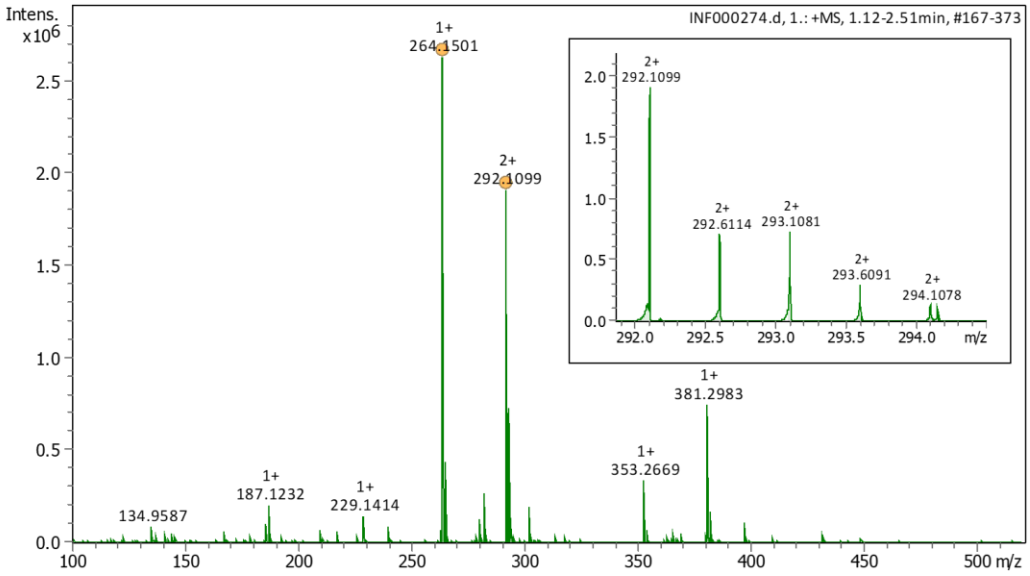

Figure S7. Experimental ESI–MS of **NiC1** in positive mode (calcd: m/z^{2+} = 292.1100; $[M–2PF_6^-]^{2+}$).

5. MALDI-TOF mass characterization of Ni^{II} complexes

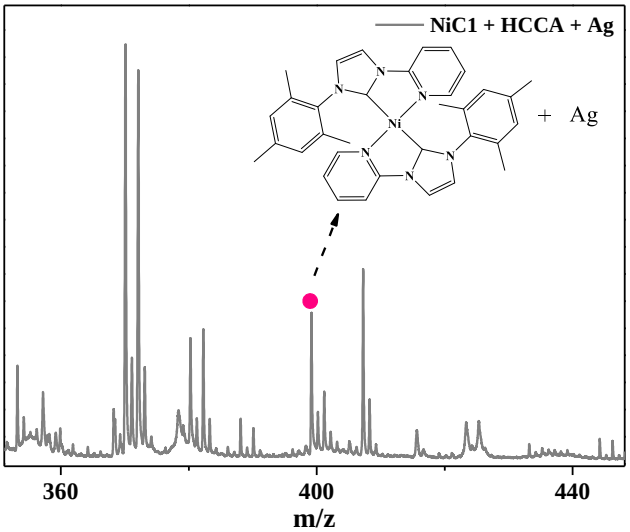

Figure S8. MALDI-TOF mass spectrum of complex **NiC1**.

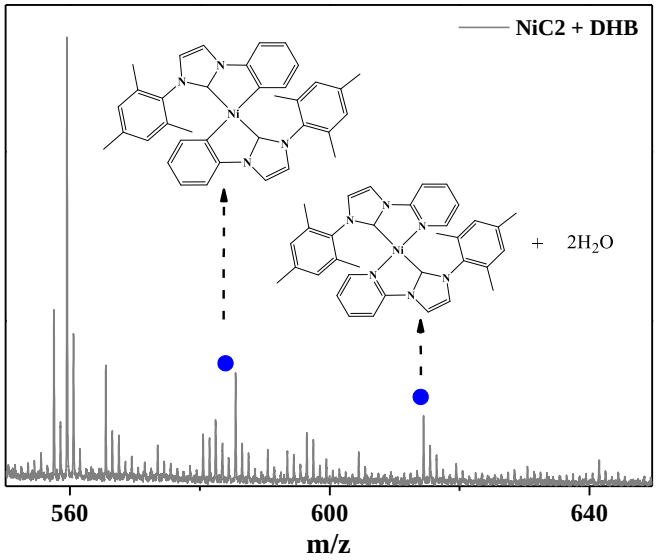

Figure S9. MALDI-TOF mass spectrum of complex **NiC2**.

6. UV-Vis characterization of Schiff-base ligands and Ni^{II} complexes

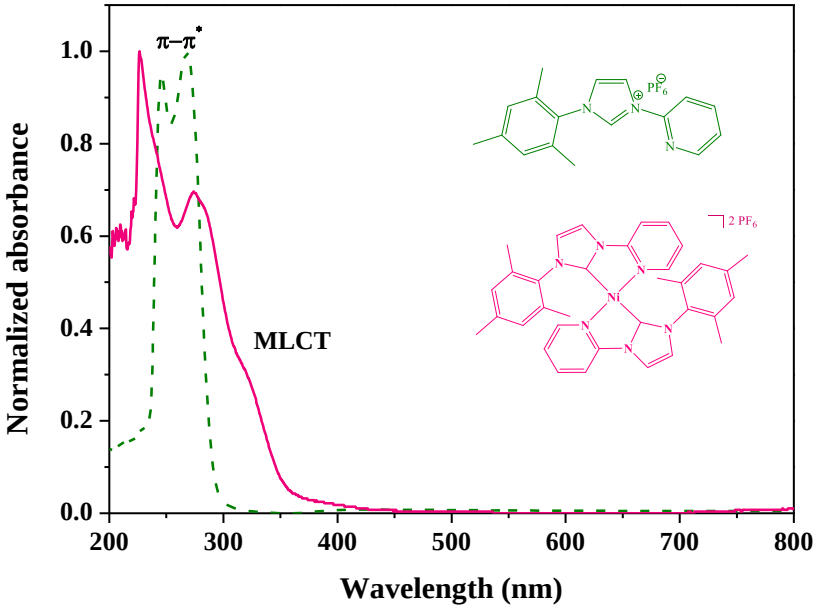

Figure S10. UV-Vis spectra for **NiC1** (solid pink line) and **HC1** (dash green line).

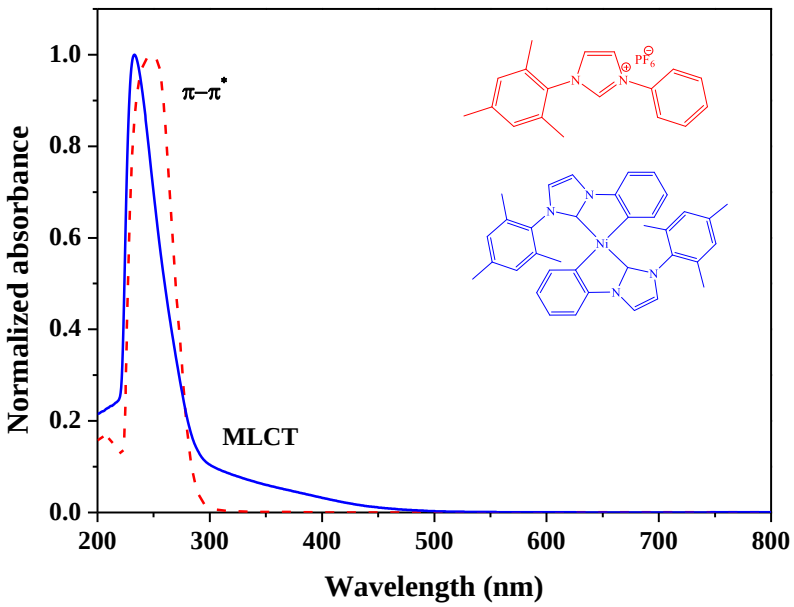

Figure S11. UV-Vis spectra for **NiC2** (solid blue line) and **HC2** (dash red line).

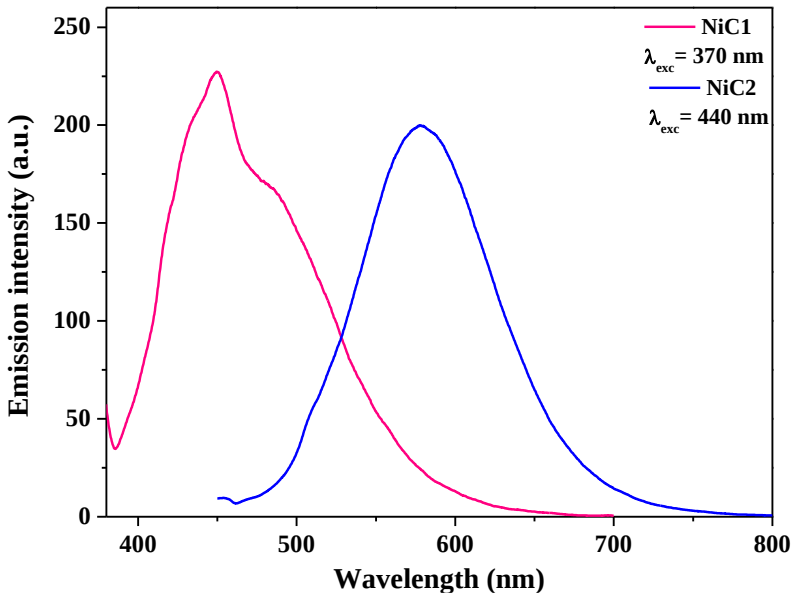

Figure S12. Emission spectra for **NiC1** (solid pink line) and **NiC2** (solid blue line).

7. Cyclic voltammetry of Ni^{II} complexes

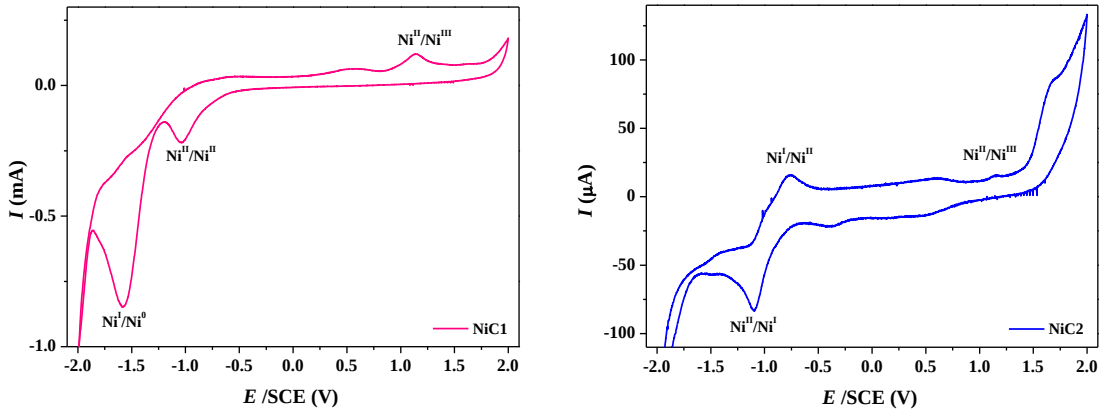

Figure S13. Cyclic voltammetry of **NiC1**, and **NiC2** from 1 × 10^{-3} mol L^{-1} in acetonitrile solutions and *n*-Bu_4NPF_6 0.1 mol·L^{-1} *vs*. SCE; obtained at 100 mV·s^{-1} at 25 °C.

8. Steady-state photolysis of the Ni^{II} complexes

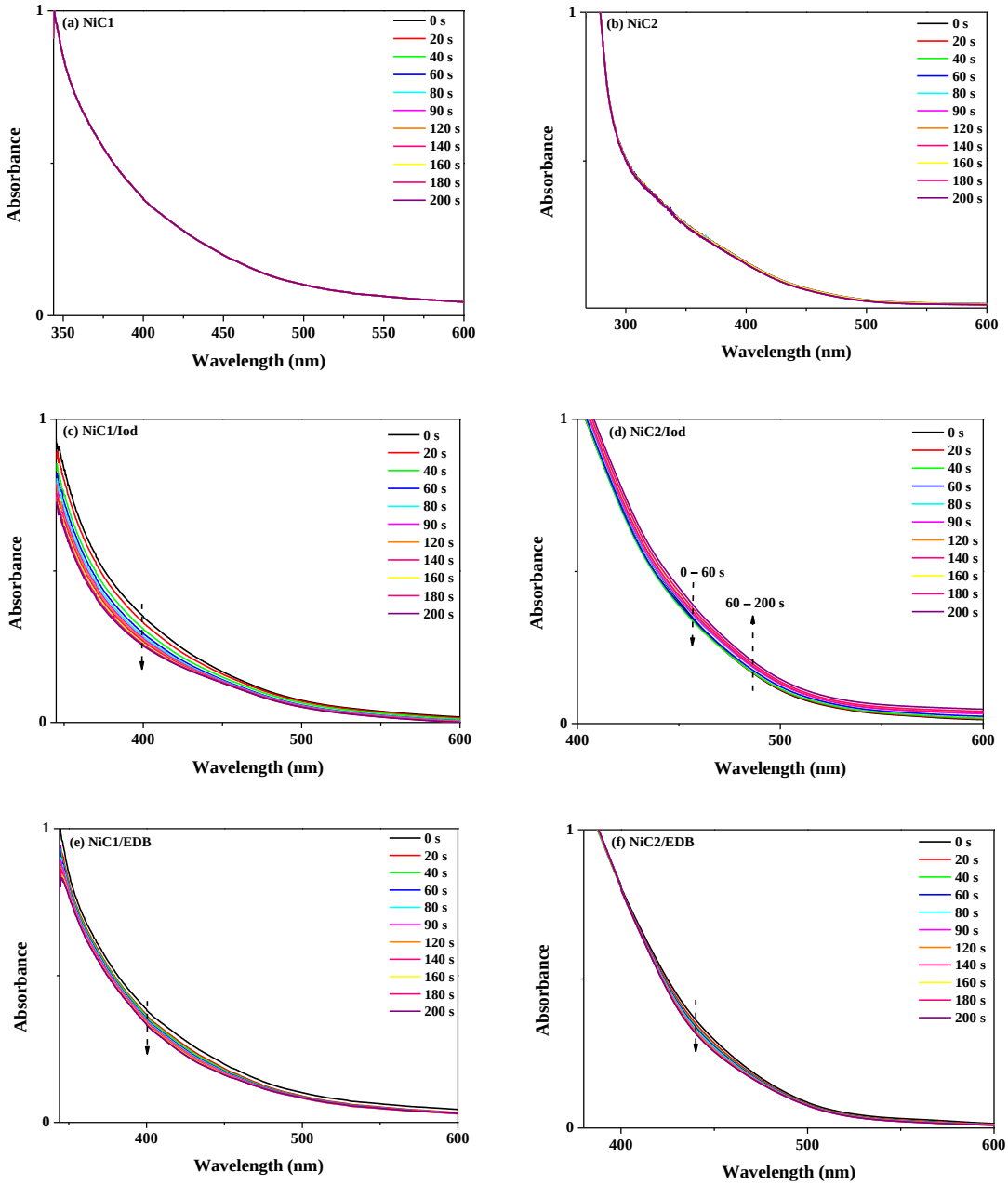

Figure S14. UV–Vis absorption spectra of **NiC1** and **NiC2** in CH_2Cl_2: (a,b) Ni^{II}, (c,d) Ni^{II}/Iod, and (d,e) Ni^{II}/EDB upon exposure under air to LED@405 nm for different times.

9. Fluorescence quenching of NiC1

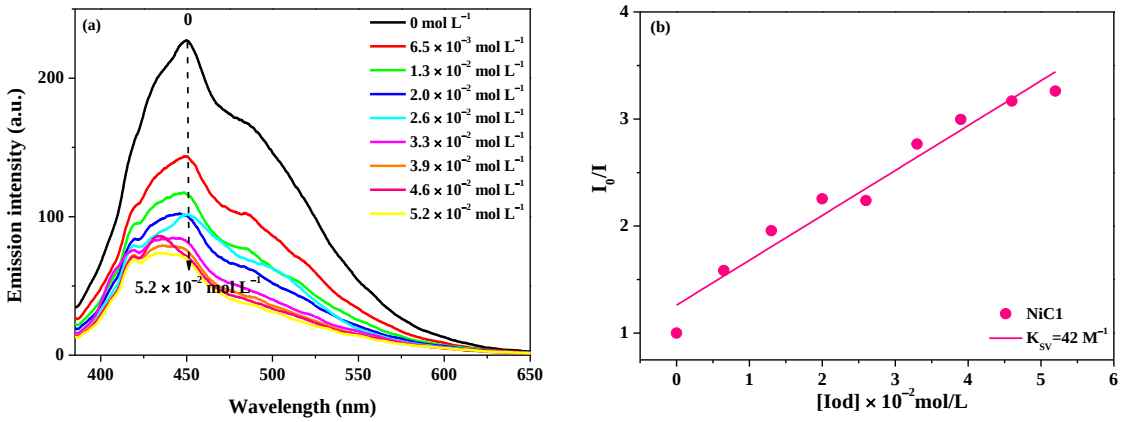

Figure S15. Fluorescence quenching of **NiC1** with additives in CH_2Cl_2: (a) **NiC1**/Iod; (b) Stern-Volmer coefficient determination with Iod.

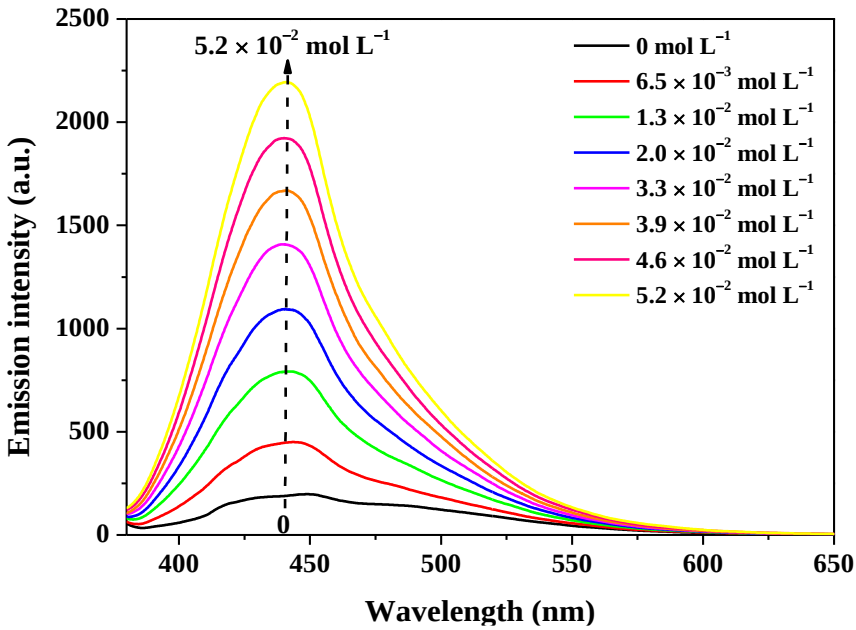

Figure S16. Emission spectra of **NiC1** with EDB in CH_2Cl_2.

10. FTIR spectra of photopolymerizations

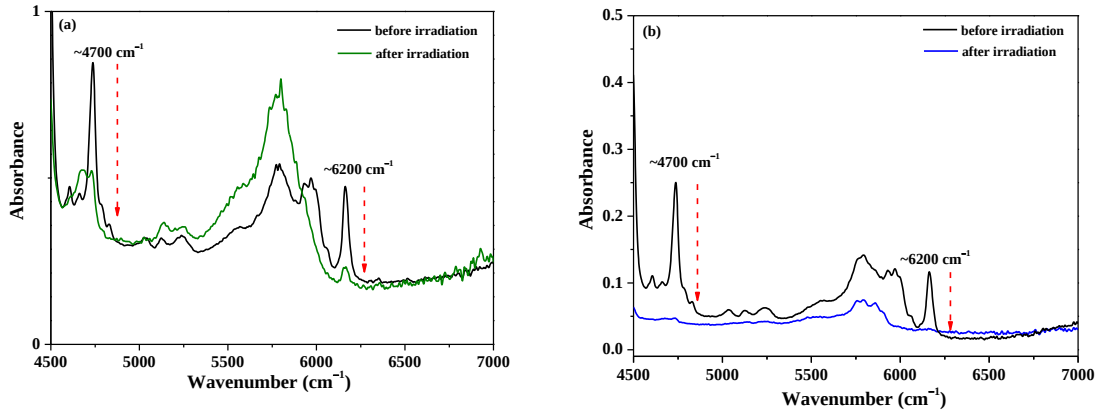

Figure S17. FTIR spectra recorded before and after photopolymerization for 0.2%/2%/2% w/w/w **NiC2**/Iod/EDB under LED@405 nm. (a) under pallet; (b) in laminate.

11. ESR spin-trapping experiments of NiC1

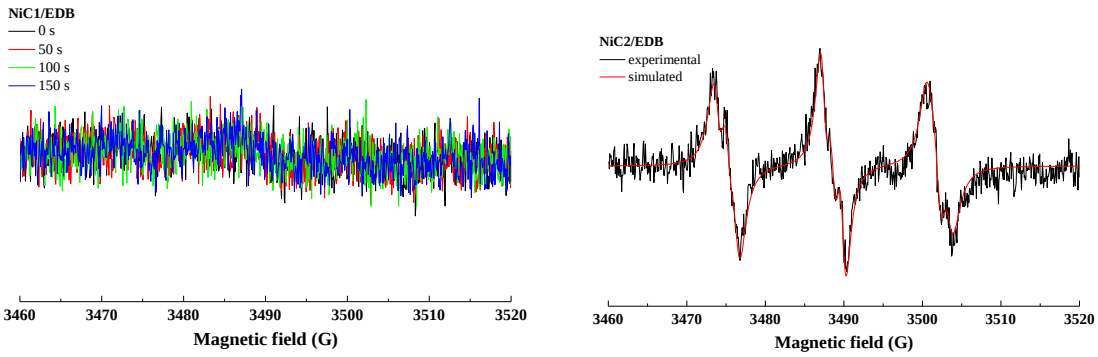

Figure S18. ESR spectra obtained from ESR-spin trapping experiments under LED@405 nm using PBN = 5×10^{-2} mol L^{-1} (as the spin trap agent); EDB = 1×10^{-2} mol L^{-1}, and Ni^{II} = 1×10^{-3} mol L^{-1} in CH_2Cl_2.

1 N. M. Pesqueira, F. Morlet-Savary, M. Schmitt, V. P. Carvalho-Jr, B. E. Goi and J. Lalevée, *Eur Polym J*, 2024, **216**, 113279.